Determining complete electron flow in the cofactor photoreduction of oxidized photolyase

Zheyun Liu[a,b], Chuang Tan[a,b,c], Xunmin Guo[a,b], Jiang Li[a,b], Lijuan Wang[a,b], Aziz Sancar[d,1], and Dongping Zhong[a,b,c,e,f,1]

Departments of [a]Physics and [b]Chemistry and Biochemistry, and Programs of [e]Biophysics, [c]Chemical Physics, and [f]Biochemistry, Ohio State University, Columbus, OH 43210; and [d]Department of Biochemistry and Biophysics, University of North Carolina School of Medicine, Chapel Hill, NC 27599

Contributed by Aziz Sancar, June 25, 2013 (sent for review May 25, 2013)

The flavin cofactor in photoenzyme photolyase and photoreceptor cryptochrome may exist in an oxidized state and should be converted into reduced state(s) for biological functions. Such redox changes can be efficiently achieved by photoinduced electron transfer (ET) through a series of aromatic residues in the enzyme. Here, we report our complete characterization of photoreduction dynamics of photolyase with femtosecond resolution. With various site-directed mutations, we identified all possible electron donors in the enzyme and determined their ET timescales. The excited cofactor behaves as an electron sink to draw electron flow from a series of encircling aromatic molecules in three distinct layers from the active site in the center to the protein surface. The dominant electron flow follows the conserved tryptophan triad in a hopping pathway across the layers with multiple tunneling steps. These ET dynamics occur ultrafast in less than 150 ps and are strongly coupled with local protein and solvent relaxations. The reverse electron flow from the flavin is slow and in the nanosecond range to ensure high reduction efficiency. With 12 experimentally determined elementary ET steps and 6 ET reaction pairs, the enzyme exhibits a distinct reduction–potential gradient along the same aromatic residues with favorable reorganization energies to drive a highly unidirectional electron flow toward the active-site center from the protein surface.

protein electron transfer | flavin photoreduction | femtosecond dynamics | electron flow directionality | reduction potential funnel

Photolyase and cryptochrome are evolutionally related and contain a flavin adenine dinucleotide (FAD) as the catalytic cofactor with a unique bent structure in the active sites, but the two perform different functions: photolyase repairs UV-damaged DNA and cryptochrome functions as a photoreceptor for regulation of plant growth or synchronization of circadian rhythm (1–5). The active state of the cofactor in vivo is in the anionic hydroquinone form ($FADH^-$) in photolyase (6), but currently the redox status of flavin in cryptochrome is under debate with some studies suggesting flavin to be in oxidized (FAD), whereas others claiming anionic (FAD^-/$FADH^-$) states for the functional form in vivo (7–10). However, in vitro, the cofactor is oxidized to FAD and/or $FADH^•$ in photolyase but only appears in the oxidized FAD state in cryptochrome. Thus, it appears that reduction of the oxidized FAD is necessary for its transformation into the active state. Photoinduced electron transfer (ET) is an effective way for such redox state changes and it is conceivable that the photoreduction of FAD could be a primary process for signal initiation in cryptochrome (11).

In this study, we used *Escherichia coli* photolyase (EcPL) as a model system for systematic studies of electron flow into the excited cofactor FAD. As shown in Fig. 1, more than 10 aromatic acid residues (W and Y) encircle the flavin cofactor around the active site (12). These aromatic residues not only are critical to structural integrity (13) but also are rich electron donors (7). The electrons can flow into the excited cofactor in multiple unidirectional pathways and the cofactor behaves as an electron sink to draw surrounding electrons from multiple layers of aromatic residues (Fig. 1). Earlier biochemical studies (14) as well as X-ray structures (12) identified the conserved tryptophan triad (W382, W359, and W306) as the main electron source for photoreduction, and the recent ultrafast studies (15–17) of semiquinone $FADH^•$ photoreduction revealed the continuing hopping mechanism along the tryptophan triad. The hopping mechanism, consisting of multiple tunneling steps, has been shown to significantly accelerate electron transport in DNA (18) and also recently in proteins (19). Here, we examine all possibilities of electron flow from various electron donors in photoreduction of FAD in photolyase, and we report the observation of ET reactions involving the adenine moiety in addition to the other two W384 and W316 aromatic residues. With femtosecond spectroscopy, we resolved the dynamics of all elementary ET steps and determined their timescales. We further evaluated the reduction potentials and reorganization energies (λ) in each tunneling ET step. Modulated by the protein environment, the cluster of tryptophans was found to have a reduction–potential gradient that drives the efficient multiple tunneling steps in a hopping pathway with distinctive directionality to FAD in photolyase.

Results and Discussion

All experiments were conducted on photolyase E109A mutant template. This mutation abolished binding of the folate antenna chromophore, without affecting the structure or catalytic mechanism of the enzyme and hence enabling analyses of the flavin dynamics by absorption spectroscopy without interference from a second chromophore. For simplicity, we will refer to the E109A mutant as "wild type." All other mutants were made on this template. To dissect the complex ET networks and isolate each electron flow channel, based on X-ray structures, we prepared three single-position mutants of W382F, W359F, and W306F and two double-position mutants of W382F/W384F and W316F/W359F. Fig. 2 shows the striking patterns of the femtosecond absorption transients of the wide type and one of three tryptophan-triad mutants, probed at 10 different visible wavelengths from 800 to 450 nm. For example, all signals decay to zero in less than 1 ns for the mutant of W382F, indicating that all ET reactions are completed on such timescales. For the wild type and W306F mutant (Fig. S1), the signals probed at the longer wavelengths decay to zero but at the shorter wavelengths stay longer than 3 ns. By systematic analyses of these transients (*SI Text*), we can resolve the dynamics of each individual ET channel, determine the electron flow directionality, and finally elucidate the nature of these ET reactions as detailed below.

Author contributions: D.Z. designed research; Z.L., C.T., X.G., J.L., L.W., and D.Z. performed research; Z.L., C.T., X.G., J.L., and D.Z. analyzed data; and Z.L., A.S., and D.Z. wrote the paper.

The authors declare no conflict of interest.

Freely available online through the PNAS open access option.

[1]To whom correspondence may be addressed. E-mail: dongping@mps.ohio-state.edu or aziz_sancar@med.unc.edu.

This article contains supporting information online at www.pnas.org/lookup/suppl/doi:10.1073/pnas.1311073110/-/DCSupplemental.

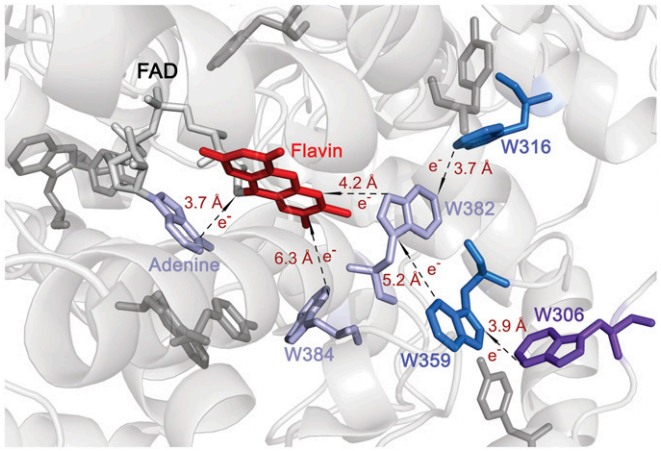

Fig. 1. ET networks in photolyase with all tunneling distances shown. The flavin moiety of FAD (red) behaves as an electron sink to draw electron flow from a series of aromatic molecules. The adenine moiety, W384 and W382 (light blue), have direct ET with flavin in the first layer, whereas the W316 and W359 (dark blue) form the second layer having direct ET with W382. The third-layer W306 (purple) is exposed to the protein surface. All other aromatic residues of tryptophan and tyrosine (gray) near the ET networks are also shown.

Identifying New Electron Donors (Ade and W384) in Initial Electron Injection. With the double-position mutations of W382 and W384 to redox-inert phenylalanine (W382F/W384F), we eliminated all aromatic W and Y residues within 7 Å in the first layer from the cofactor flavin. Fig. 3 *A* and *B* show two typical absorption transients of this mutant from our 10-wavelength detections. Without any nearby aromatic W and Y residues, the excited FMN* and FAD* with an open configuration in proteins have a lifetime of several nanoseconds (20). In water, FAD is in a dynamic equilibrium between two conformations, stacked and open. The excited FAD has a lifetime of 2.5 ns for the open structure but has an ultrafast lifetime of 9 ps with the stacked configuration due to intramolecular ET from the adenine moiety to the isoalloxazine ring (20). Thus, the ultrafast decay in Fig. 3*A* must represent an ET quenching by the neighboring adenine at 3.7 Å with the bent U-shape configuration. After the charge separation, the cation Ade^+ has wide absorption in the visible region. By systematic fitting of the 10 transients with three states (Fig. 3*C*), we obtained the excited FAD decay in 18 ps (dominant in Fig. 3*A* probed at 800 nm) and the intermediate Ade^+ decay in 96 ps (in Fig. 3*B* at 580 nm also with a negative absorption signal of the stimulated emission of FAD* in 18 ps) with a stretched parameter (β) of 0.92. We have to emphasize that the ET reactions are coupled with active-site relaxation. We have measured the active-site solvation dynamics in the reduced $FADH^-$ state and have found that the relaxation takes place on the timescales from a few picoseconds to subnanoseconds (21). The similar timescales would be expected for the oxidized FAD state (22) and therefore the ET dynamics shows a stretched behavior, $Ae^{-(t/\tau)^{\beta}}$, where A is the amplitude, τ is the lifetime, and β here is a stretched parameter. Using $<\tau> = \frac{\tau}{\beta}\Gamma\left(\frac{1}{\beta}\right)$, we obtained the average lifetimes of the forward ET in 19 ps and the back ET in 100 ps (Fig. 3*C*); all ET times in photolyase thereafter will be the averaged ones over the stretched behavior. The results observed here are consistent with the dynamics of FAD* in aqueous solution with a stacked configuration, the forward ET in about 9 ps and the back ET in about 35 ps (20). This observation unambiguously ensures that the intramolecular ET reaction also occurs in the $FADH^{\bullet}$ state, suggesting that an earlier report of 80 ps for the intrinsic lifetime of $FADH^{\bullet}$* or the ET reaction with W359 (23) actually includes the ET dynamics with the adenine moiety. Hence, the adenine moiety in the bent U-shape structure is an ideal electron donor. In photolyase, we have recently found that the adenine has a functional role and mediates ET for the DNA repair (24). Thus, the adenine in the bent structure of the flavin cofactor in photolyase and cryptochrome could have multiple functional roles.

Besides the nearby intramolecular adenine, two tryptophan residues, W382 and W384, are also close to the isoalloxazine ring at the distances of 4.2 and 6.3 Å, respectively. With the single mutant W382F, we isolated the ET flow only from adenine and W384. At 800 nm, the transient has a dominant decay in 15 ps (Fig. 3*D*), faster than that of W382F/W384F mutant (Fig. 3*A*), reflecting the total quenching of FAD* from the two parallel ET pathways, the adenine and W384 (Fig. 3*F*), and giving a forward ET time of 80 ps from W384 to FAD*. Although tryptophan is a better electron donor than adenine, the longer separation distance with the isoalloxazine ring leads to a smaller electronic coupling constant and thus a slower ET rate. At 580 nm, we detected both intermediates of Ade^+ and $W384^+$ cationic radicals (Fig. 3*E*). By knowing the ET dynamics with adenine, we determined the dynamics of back ET for $W384^+$ in about 120 ps (Fig. 3*F*), and the resulting relative absorption coefficients of Ade^+ and $W384^+$ are also consistent with those in aqueous solution (25, 26).

Determining Dominant Electron Flow (W382) and Subsequent Second-Layer Donors (W316 and W359). Knowing the ET dynamics with Ade in 19 ps and W384 in 80 ps, we further studied the double mutations of W316F/W359F and determined the ET dynamics with W382. We obtained the forward ET in 0.8 ps and back ET in 70 ps (Fig. 3*I*), similar to our earlier report (7). Thus, in the initial electron flow, the dominant channel is W382 with a branching of 0.95. Significantly, the back ET is very slow, leaving enough time

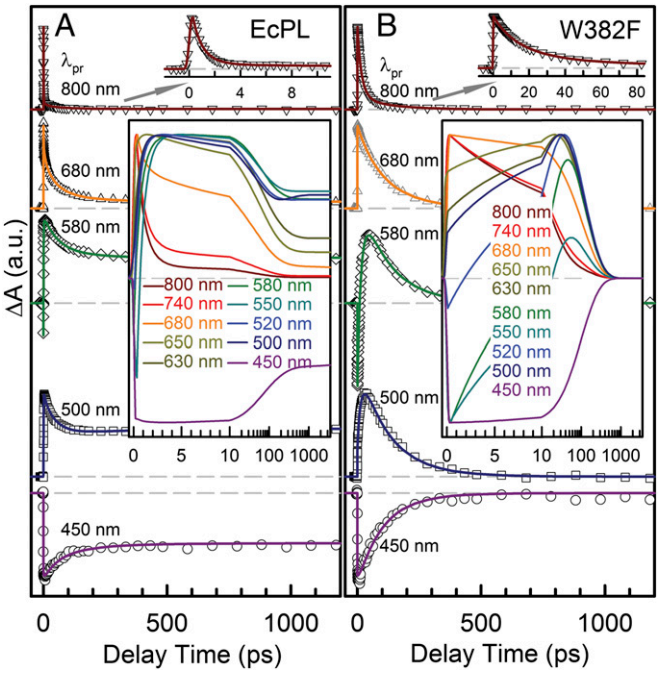

Fig. 2. Femtosecond-resolved transient absorption dynamics of photoreduction of various mutants: (*A*) Wild type (E109A mutant); (*B*) W382F. The photoreduction dynamics are probed systematically from 800 to 450 nm and several typical results are shown with a distinct pattern. *Upper Insets* are the results probed at 800 nm with a short time window. *Lower Insets* show the fitting curves with 10 probing wavelengths from 800 to 450 nm, and the results are plotted by a linear scale before 10 ps and by a logarithmic scale after 10 ps.

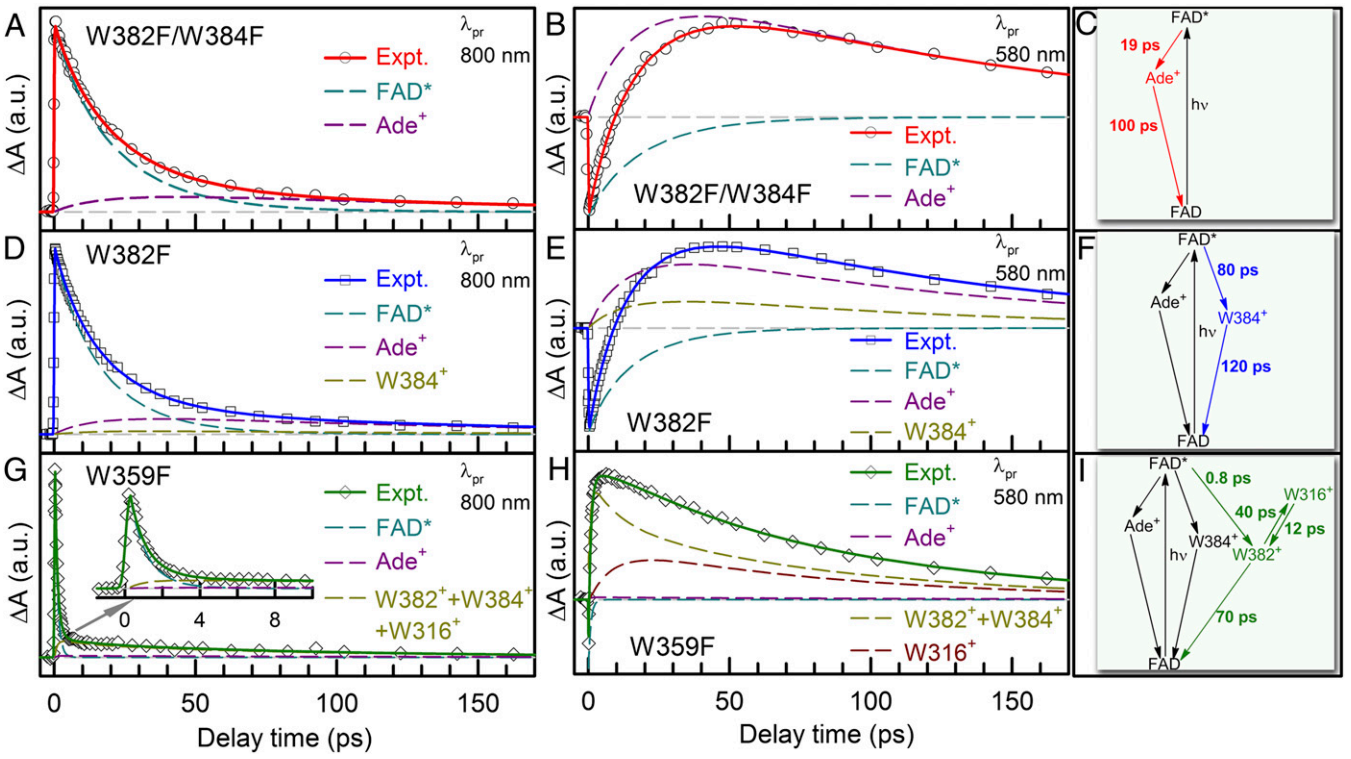

Fig. 3. Femtosecond-resolved ET dynamics of flavin with the first-layer adenine moiety, W384 and W382, and of W382 with the second-layer W316. (*A* and *B*) Normalized transient absorption signals of W382F/W384F mutant probed at 800 and 580 nm, respectively, with the decomposed dynamics of the reactant (FAD*) and intermediate (Ade^+). (*C*) Shown are the obtained ET dynamics between flavin and adenine moiety (red arrows). (*D* and *E*) Normalized transient absorption signals of W382F mutant probed at 800 and 580 nm, respectively, with the decomposed dynamics of the reactant (FAD*) and intermediates (Ade^+ and $W384^+$). (*F*) Shown are the obtained ET dynamics between flavin and W384 (blue arrows). (*G* and *H*) Normalized transient absorption signals of W359F mutant probed at 800 and 580 nm, respectively, with the decomposed dynamics of the reactant (FAD*) and various intermediates (Ade^+, $W384^+$, $W382^+$, and $W316^+$). (*I*) Shown are the obtained ET dynamics of flavin with W382 and of W382 with W316 (dark green arrows).

for electrons to continue flowing from the second donor layer of W316 and W359 (equivalently a hole transfer from $W382^+$ to the second layer of W316 and W359) and significantly enhancing the photoreduction efficiency. With the mutant of W359F to leave W316 alone in the second layer, we are able to examine the ET dynamics of two aromatic tryptophans between $W382^+$ and W316. Similar to the double mutant W316F/W359F, we first observed the initial ET flow in 0.8 ps (Fig. 3*G*). In addition to the longtime decay of tryptophan cation, we also observed a rise time of around 10 ps (Fig. 3*H*). By the systematic analyses of 10 transients (Fig. S2), we resolved the dynamics of forward ET in 40 ps and back ET in 12 ps (Fig. 3*I*). The observation reflects that W316 significantly branches out the electron flow (hole transfer) and effectively delays the complete charge recombination between $W382^+$ and the cofactor to leave FAD^- for a longer time.

With the understanding of the ET dynamics with W316, we studied the mutant W306F to further examine the electron flow from W359 in the second layer. Significantly, we observed very different transient dynamics at the longer time (especially around 510 nm in *Inset* of Fig. S1) and the signals stay longer than 3 ns out of our time window. Specifically, from the early decay of tryptophan cation in 100–200 ps probed at 580 nm (Fig. 4*B*), we determined the forward ET between $W382^+$ and W359 also in about 70 ps (Fig. 4*A*). Around 510 nm, the observed increasing signals (*Inset* in Fig. S1 and Fig. 4*C*), especially at the longer time of >1 ns, are from the deprotonated $W359^+$ ($W359^\bullet$), as also observed in the $FADH^\bullet$ photoreduction (17). The N1 atom of $W359^+$ is within hydrogen bond distance to a water molecule, facilitating the deprotonation process and thus stabilizing the neutral $W359^\bullet$ radical. Thus, the observed longtime decay in nanoseconds must be from the dynamics of $W359^+$ and represents the total rate of the back ET from W382 and deprotonation to $W359^\bullet$ (Fig. 4 *B* and *C*). By knowing the relative absorption coefficients of W^+ and $W^\bullet$ (15), we derived the back ET in 1.2 ns and the deprotonation in 3 ns (Fig. 4*A*). The faster forward ET (70 ps) and slower back ET (1.2 ns) with W359 ensure the electron flow (hole transfer) gradient and enable the $W359^+$ cation (or hole) to stay longer to keep electron flow from the third-layer W306. Also, the 3.0-ns deprotonation time is similar to the reported value in $FADH^\bullet$ photoreduction (17) so that the acidity surrounding W359 does not change between the two redox states of flavin (FAD and $FADH^\bullet$).

Characterizing Terminal Electron Donor (W306) and Completing Photoreduction Cycle. With the understanding of electron flow in the second layer, we studied the ET dynamics of the wild type that contains the entire ET networks with the terminal electron donor W306 in the outer third layer on the protein surface that is exposed to the solvent. Comparing with the transients from the W306F mutant (*Insets* in Fig. 2*A* and Fig. S1), we observed less amplitude of the decay component in 100–200 ps detected in the region of 650–500 nm (Fig. 5*B* at 580 nm) and a rise component in hundreds of picoseconds at 500 nm (Fig. 5*C*). By systematic fitting, we unambiguously differentiated the signal of $W306^+$ from the other tryptophan cations (Fig. 5 *B* and *C*, dashed orange lines) and obtained the forward ET dynamics from W306 to $W359^+$ in 150 ps (Fig. 5*A*). Such forward ET dynamics in 150 ps was also observed in our anisotropy studies (Fig. S3). Significantly, the forward ET from the third-layer W306 to $W359^+$ is much faster than the back ET from the first-layer W382 (1.2 ns) and its

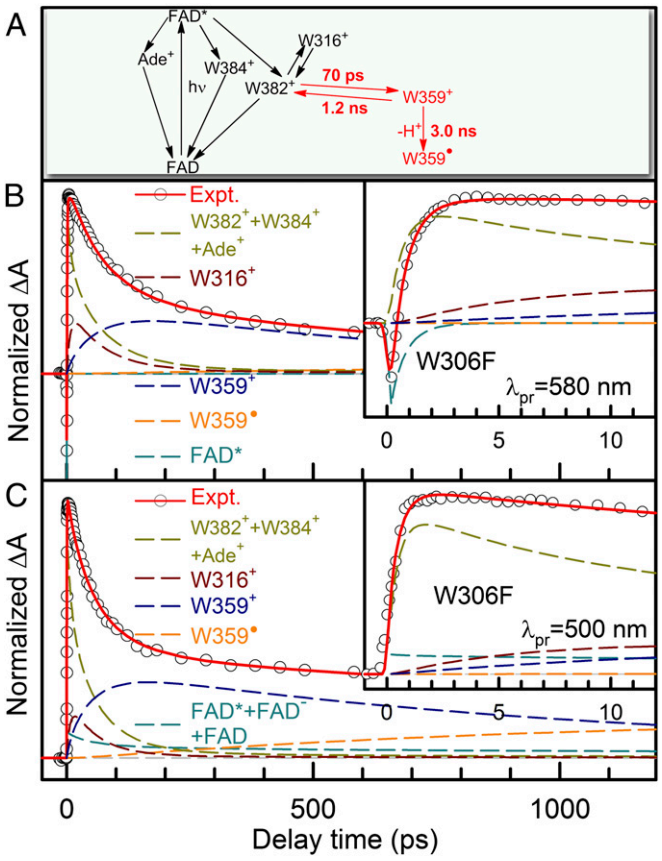

Fig. 4. Femtosecond-resolved ET dynamics of the second-layer W359 with W382. (*A*) Shown are the obtained ET dynamics between W359 and W382 and the deprotonation process of cationic W359 radical (red arrows). (*B* and *C*) Normalized transient absorption signals of W306F mutant probed at 580 and 500 nm with the decomposed dynamics of the reactant (FAD*) and various intermediates (Ade^+, $W384^+$, $W382^+$, $W316^+$, $W359^+$, and $W359^•$, and FAD^-) and product (FAD). *Insets* show the dynamics in the short time range.

deprotonation (3 ns), and thus this forward step has a very high branching ratio of 0.85, leading to the efficient electron flow from the third layer. The resulting $W306^+$ has no obvious decay behavior (Fig. 5 *B* and *C*) within our 4-ns time window and we estimated a lower limit of 100 ns for the back ET from W359 (Fig. 5*A*). Thus, the $W306^+$ cation stays for a quite long time, making the further reduction of its deprotonation readily (15). We did not observe any ET dynamics with the Y464 residue at a distance of 3.7 Å from W306, indicating that this process, if any, should occur at a much longer timescale.

With the third-layer W306 as the terminal electron donor located at the protein surface, the photoreduction is completed. Strikingly, these ET tunneling steps in picoseconds are much faster than the reverse processes in nanoseconds. The dominant electron flow through the conserved tryptophan triad (W384, W359, and W306) is efficient, reaching a quantum yield of about 0.4. For three chemically identical residues of the tryptophan triad, their redox properties must be different. The W382 and W359 residues are buried inside the protein, whereas W306 is at the loop region and exposed to surface to interact with bulk water directly. Therefore, W306 is in a high dielectric medium with a hydrophilic environment so that the potency of $W306^+$ to hold a positive charge is largest, leading to the lowest reduction potential. Between W382 and W359, more hydrophilic residues and two structured water molecules surround the latter, resulting in a lower reduction potential for W359. Thus, the reduction potentials of three conserved tryptophans appear in an increasing order: $E°(W306^+/W306) < E°(W359^+/W359) < E°(W382^+/W382)$. The three conserved tryptophan residues with the different environments also result in the variation of their cation absorption (Fig. S4).

Reduction–Potential Gradient, Reorganization Energy Locality, and Electron Flow Directionality. By determining the dynamics and timescales of more than 12 individual ET steps in photoreduction of FAD (Fig. 6*A*), we identified all electron tunneling channels and ET donors involved in the three layers including the adenine moiety, W384 and W382 as the primary electron tunneling, then W316 and W359 as the secondary step to continuously flow electrons to W382, and finally W306 as the terminal electron donor connecting to the protein surface for the complete reduction. The conserved tryptophan triad is the dominant electron flow route with a multistep tunneling mechanism. For all these 12 determined ET steps, electron tunnels between the donor and acceptor through a superexchange mechanism. Thus, we can apply the empirical Marcus ET formula to further understand the ET mechanism (27):

$$\log k_{ET} = 13 - 0.434\,\beta(r - r_0) - 3.1\left(\Delta G^0 + \lambda\right)^2/\lambda, \qquad [1]$$

where k_{ET} is the ET rate in seconds^{-1}, β here is the empirical ET parameter in angstroms^{-1}, r is the edge-to-edge separation distance in angstroms, r_0 is the van der Waals distance at 3.0 Å,

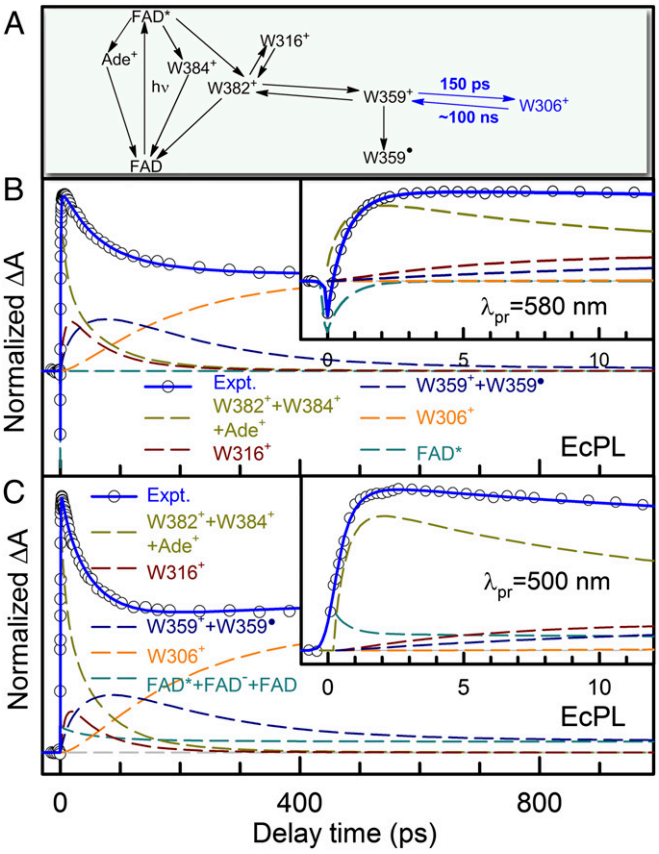

Fig. 5. Femtosecond-resolved ET dynamics of the third-layer W306 with W359. (*A*) Shown are the obtained ET dynamics between W306 and W359 (blue arrows). (*B* and *C*) Normalized transient absorption signals of the wild type (E109A) probed at 580 and 500 nm with the decomposed dynamics of the reactant (FAD*), various intermediates (Ade^+, $W384^+$, $W382^+$, $W316^+$, $W359^+$, $W359^•$, $W306^+$, and FAD^-) and product (FAD).

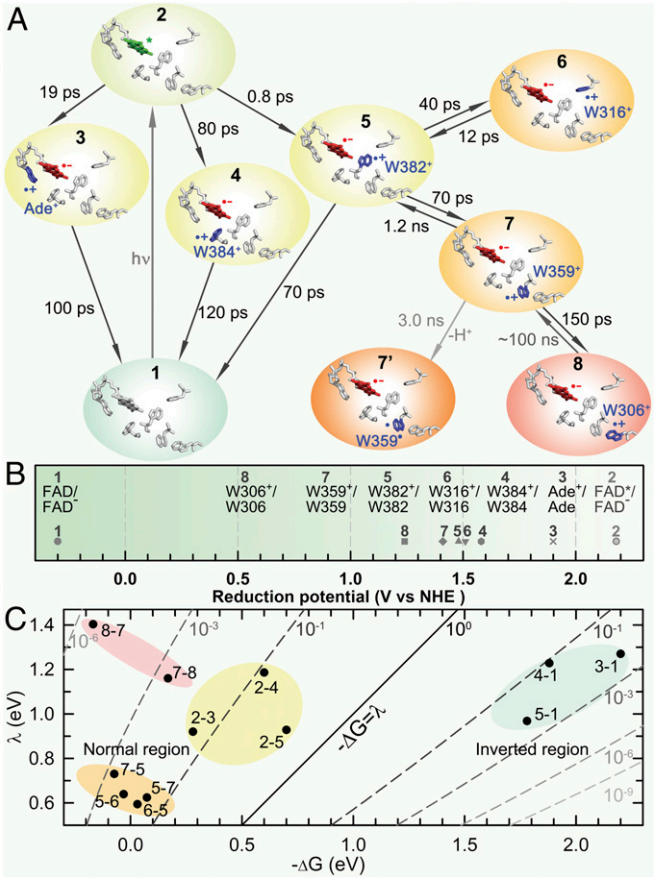

Fig. 6. Summary of 12 ET dynamics of photoreduction of oxidized flavin within 6 ET reaction pairs in photolyase and their dependence on driving forces and reorganization energies. (*A*) Dynamics and timescales of all elementary steps including 12 ET reactions (with hole transfer directions) and one deprotonation process with the charge location for each ET step. (*B*) The derived reduction potentials of all seven electron donors and acceptors. (*C*) Two-dimensional plot of the Franck–Condon (energy) parts of ET rates relative to free energy (ΔG^0) and reorganization energy (λ) for all 12 electron tunneling steps (taking β = 1.4 Å^{-1} as an example). The three charge-recombination steps with flavin fall in the Marcus inverted ET region ($-\Delta G^0 > \lambda$) and all other ET reactions in the Marcus normal region ($-\Delta G^0 \leq \lambda$). The Franck–Condon parts of ET rates are modulated by both driving force and reorganization energy. The overall efficiency of photoreduction is maximized by the ultrafast unidirectional electron flow from W306 toward the active site (2-5, 5-7, and 7-8) and the "ultraslow" charge-recombination processes (5-1, 7-5, and 8-7).

ΔG^0 is the total free energy in electron volts, and λ is the reorganization energy in electron volts (eV). The β value mostly ranges from 1.0–1.4 Å^{-1} in proteins to 1.55–1.65 Å^{-1} in water (28).

Knowing the forward and backward tunneling rates between the four tryptophans of W306, W359, W382, and W316 (Fig. 6*A*), we obtained the free energy changes (ΔG^0) of −168, −73, and 31 meV, respectively, for these ET steps from W306 to W359 and then to W382, and from W316 to W382 (Fig. 1). On the other side, by knowing the excitation energy of 2.48 eV through the $S_1 \leftarrow S_0$ transition around 500 nm, considering a larger reorganization energy for the backward ET than the forward ET, and combining both the forward and backward ET dynamics using Eq. **1**, we derived the most feasible free energy around −0.7 eV for the dominant ET between FAD* and W382. The reduction potential of FAD/FAD$^-$ in aqueous solution is about −0.3 V vs. normal hydrogen electrode (NHE) (29), and thus the minimum reduction potential of W382$^+$/W382 is 1.48 V vs. NHE. Therefore, we derived the reduction potentials of 1.51, 1.41, and 1.24 V vs. NHE for W316, W359, and W306 (Fig. 6*B* and Table S1), respectively. The derived reduction potential of 1.24 V for W306$^+$/W306 is larger than that of tryptophan in aqueous solution, 1.15 V vs. NHE (30), consistent with its surface-exposed position with a less aqueous environment. Clearly, along the tryptophan triad, a strong reduction–potential gradient exists from the higher W382 to lower W306, driving unidirectional electron flow from W306 to W382 and resulting in ultrafast cascade ET dynamics. Using Eq. **1**, with the β values in 1.0–1.6 Å^{-1}, we obtain the reorganization energies of 1.21–1.13 eV for the forward and of 1.45–1.38 eV for the backward ET from W306 to W359$^+$. However, for W359 to W382$^+$, the reorganization energies decrease to 0.75–0.56 and 0.86–0.67 eV, and for W316 to W382$^+$, they are slightly lower to 0.68–0.62 and 0.63–0.57 eV, respectively. The three various reorganization energies reflect their locality, i.e., the different environments for these ET reactions in three layers. For the electron tunneling from W306 to W359$^+$, the large reorganization energy is due to the surface exposure of the third-layer W306 to bulk solvent. The similar small reorganization energies in the second layer from both W359 and W316 to W382$^+$ result from the buried, less hydrophilic local surroundings (12). All these ET tunneling processes, forward and backward, between different tryptophans are in the Marcus normal region ($-\Delta G^0 < \lambda$).

We further evaluate the driving forces and reorganization energies of the ET processes in the first layer with the cofactor flavin. Combining the forward and recombination dynamics with a larger reorganization energy for the backward ET than the forward ET for typical photoinduced ET reactions, we derived a free energy around −0.6 eV between FAD* with W384, leading to a reduction potential around 1.58 V for W384$^+$/W384 and reorganization energies of 1.31–1.06 eV for the forward and 1.16–1.30 eV for the backward for β = 1.2–1.6 Å^{-1}. Similarly, we obtained the reorganization energies of 1.00–0.84 eV for the forward and 0.95–0.98 eV for the backward of the dominant ET between FAD* and W382. For the intramolecular ET with adenine, our earlier studies showed an effective tunneling parameter of β = 0.833 Å^{-1} for electron transfer from FADH^{-*} to damaged DNA (thymine dimer) mediated by the intervening adenine moiety (24), and thus taking β = 0.833–1.4 Å^{-1}, we obtained a free energy around −0.28 eV, leading to a reduction potential of 1.9 V for Ade$^+$/Ade, consistent with the reported value of 1.96 V in aprotic solvent (31), and the reorganization energies of 1.04–0.92 and 1.22–1.27 eV for the forward and recombination, respectively. The larger reorganization energies observed in the first-layer ET is due to the highly polar active site with many trapped water molecules, similar to the ET reaction with W306, and more important, the larger inner-sphere reorganization energy from the structural distortion of FAD to FAD$^-$ (7). Clearly, in the first layer of ET, the charge separation is in the Marcus normal region and the charge recombination is in the Marcus inverted region (Fig. 6*C*).

Fig. 6*C* shows a 2D plot of the Franck–Condon (energy) parts of 12 ET tunneling steps, relative to both free energy (ΔG^0) and reorganization energy (λ) (Table S2). Such a plot is rather informative and clearly shows the normal and inverted regions and the Franck–Condon parts of ET rates in function of both driving force and reorganization energy. The derived ET values of free energies and reorganization energies from Eq. **1** are under assumption of equilibrium ET processes, and clearly these ET dynamics reported here are in nonequilibrium with local protein and solvent relaxations due to the overlap of timescales between ET dynamics and active-site relaxation (21). Woiczikowski et al. (32) recently reported nonadiabatic quantum mechanics/molecular mechanics simulations of these ET dynamics and also showed the nonequilibrium nature of these tunneling processes. The calculated reorganization energies for ET among the conserved

tryptophan triad are similar to those we obtained here. The more accurate calculations can be done using the Sumi–Marcus 2D ET model (33) or the theoretical method recently developed by Matyushov that was used to treat the ET dynamics in photosynthesis (34) and such work is currently under way.

Conclusion

We reported here our systematic characterization of the photoreduction dynamics of oxidized cofactor flavin in photolyase with femtosecond transient spectroscopy and site-directed mutagenesis. With various mutations, we isolated all electron donors step by step and determined all ET dynamics, forward and backward, and their timescales. Basically, the excited cofactor behaves as an electron sink to draw electron from neighboring aromatic molecules (residues) in three successive layers to ensure electron flow from the protein surface to the active site and to complete the photoreduction cycle. We identified two electron donors (adenine and W384) in addition to the known W382 in the first layer. The intramolecular electron transfer with the adenine moiety in cofactor flavin with the bent configuration could have a potential functional role to assure the ET reaction occurring in the active site. In the second layer, we identified another electron donor (W316) in addition to the known W359. Finally, the electron flow is from the known surface W306 in the third layer.

The tryptophan triad (W382, W359, and W306) that was discovered early (12, 14, 15) is determined to be the dominant photoreduction route. The electron flow follows a hopping pathway with multiple tunneling steps. With 12 elementary ET steps we determined here, we observed a reduction–potential gradient from the active site within the core of the enzyme to the protein surface along the tryptophan triad, leading to a unidirectional electron flow from the protein surface toward the active-site center. This functional electron flow is ultrafast within 150 ps and strongly couples with the local protein fluctuations, showing clear stretched dynamic behaviors. The reverse electron flow of charge recombination is slow in nanoseconds to ensure the electron to stay in the cofactor sink and thus achieve high photoreduction efficiency. Finally, with 12 ET steps and 6 ET reaction pairs, we evaluated the reaction driving forces and reorganization energies and especially observed the strong locality of reorganization energies for the three same tryptophans, reflecting the different local dynamic motions and correlation with different surrounding protein environments.

Materials and Methods

Enzyme Preparation. The E109A mutant of *E. coli* photolyase with His-tag was prepared as described with modifications (7). To ensure the flavin cofactor in photolyase is fully oxidized, the protein is incubated in the buffer with 500 mM imidazole at 4 °C for up to 24 h before loading on a HiTrap heparin HP column (5 mL). Various mutants (W382F, W359F, W306F, W316F/W359F, and W382F/W384F) were prepared using the E109A mutant template. All proteins are stored in a reaction buffer at pH 7.5 containing 50 mM Tris·HCl, 100 mM NaCl, 1 mM EDTA, and 50% (vol/vol) glycerol. The concentration of holoprotein about 100 μM was used for experiment.

Femtosecond Spectroscopy. All of the femtosecond-resolved measurements were carried out using the transient absorption method. The experimental layout has been detailed previously (16). The instrument response time is about 250 fs and the pump-probe angle was set at 54.7° (magic angle) for all isotropic measurements and at 0° (parallel) and 90° (perpendicular) for anisotropy studies. Samples were kept stirring during irradiation to avoid heating and photobleaching. All femtosecond-resolved experiments were carried out at the pump wavelength of 480 nm and under aerobic conditions.

ACKNOWLEDGMENTS. We thank Dr. Ya-Ting Kao for the initial help with experiment. This work is supported in part by National Institutes of Health Grants GM074813 and GM31082, the American Heart Association fellowship (to Z.L.), and The Ohio State University Pelotonia fellowship (to C.T. and J.L.).

1. Sancar A (2003) Structure and function of DNA photolyase and cryptochrome blue-light photoreceptors. *Chem Rev* 103(6):2203–2237.
2. Kao Y-T, Saxena C, Wang L, Sancar A, Zhong D (2005) Direct observation of thymine dimer repair in DNA by photolyase. *Proc Natl Acad Sci USA* 102(45):16128–16132.
3. Liu Z, et al. (2011) Dynamics and mechanism of cyclobutane pyrimidine dimer repair by DNA photolyase. *Proc Natl Acad Sci USA* 108(36):14831–14836.
4. Li J, et al. (2010) Dynamics and mechanism of repair of ultraviolet-induced (6-4) photoproduct by photolyase. *Nature* 466(7308):887–890.
5. Ozturk N, Selby CP, Annayev Y, Zhong D, Sancar A (2011) Reaction mechanism of *Drosophila* cryptochrome. *Proc Natl Acad Sci USA* 108(2):516–521.
6. Kavakli IH, Sancar A (2004) Analysis of the role of intraprotein electron transfer in photoreactivation by DNA photolyase *in vivo*. *Biochemistry* 43(48):15103–15110.
7. Kao Y-T, et al. (2008) Ultrafast dynamics and anionic active states of the flavin cofactor in cryptochrome and photolyase. *J Am Chem Soc* 130(24):7695–7701.
8. Song SH, et al. (2007) Formation and function of flavin anion radical in cryptochrome 1 blue-light photoreceptor of monarch butterfly. *J Biol Chem* 282(24):17608–17612.
9. Lin CT, et al. (1995) Association of flavin adenine dinucleotide with the *Arabidopsis* blue light receptor CRY1. *Science* 269(5226):968–970.
10. Bouly JP, et al. (2007) Cryptochrome blue light photoreceptors are activated through interconversion of flavin redox states. *J Biol Chem* 282(13):9383–9391.
11. Liu B, Liu HT, Zhong D, Lin CT (2010) Searching for a photocycle of the cryptochrome photoreceptors. *Curr Opin Plant Biol* 13(5):578–586.
12. Park HW, Kim ST, Sancar A, Deisenhofer J (1995) Crystal structure of DNA photolyase from *Escherichia coli*. *Science* 268(5219):1866–1872.
13. Li X, et al. (2011) *Arabidopsis* cryptochrome 2 (CRY2) functions by the photoactivation mechanism distinct from the tryptophan (trp) triad-dependent photoreduction. *Proc Natl Acad Sci USA* 108(51):20844–20849.
14. Li YF, Heelis PF, Sancar A (1991) Active site of DNA photolyase: Tryptophan-306 is the intrinsic hydrogen atom donor essential for flavin radical photoreduction and DNA repair *in vitro*. *Biochemistry* 30(25):6322–6329.
15. Aubert C, Vos MH, Mathis P, Eker APM, Brettel K (2000) Intraprotein radical transfer during photoactivation of DNA photolyase. *Nature* 405(6786):586–590.
16. Saxena C, Sancar A, Zhong D (2004) Femtosecond dynamics of DNA photolyase: Energy transfer of antenna initiation and electron transfer of cofactor reduction. *J Phys Chem B* 108(46):18026–18033.
17. Byrdin M, et al. (2010) Quantum yield measurements of short-lived photoactivation intermediates in DNA photolyase: Toward a detailed understanding of the triple tryptophan electron transfer chain. *J Phys Chem A* 114(9):3207–3214.
18. Giese B (2000) Long-distance charge transport in DNA: The hopping mechanism. *Acc Chem Res* 33(9):631–636.
19. Shih C, et al. (2008) Tryptophan-accelerated electron flow through proteins. *Science* 320(5884):1760–1762.
20. Kao Y-T, et al. (2008) Ultrafast dynamics of flavins in five redox states. *J Am Chem Soc* 130(39):13132–13139.
21. Chang C-W, et al. (2010) Ultrafast solvation dynamics at binding and active sites of photolyases. *Proc Natl Acad Sci USA* 107(7):2914–2919.
22. Chang C-W, et al. (2010) Mapping solvation dynamics at the function site of flavodoxin in three redox states. *J Am Chem Soc* 132(36):12741–12747.
23. Byrdin M, Eker APM, Vos MH, Brettel K (2003) Dissection of the triple tryptophan electron transfer chain in *Escherichia coli* DNA photolyase: Trp382 is the primary donor in photoactivation. *Proc Natl Acad Sci USA* 100(15):8676–8681.
24. Liu Z, et al. (2012) Electron tunneling pathways and role of adenine in repair of cyclobutane pyrimidine dimer by DNA photolyase. *J Am Chem Soc* 134(19):8104–8114.
25. Solar S, Getoff N, Surdhar PS, Armstrong DA, Singh A (1991) Oxidation of tryptophan and N-methylindole by $N_3^{\bullet}$, $Br_2^{\bullet-}$, and $(SCN)_2^{\bullet-}$ radicals in light- and heavy-water solutions: A pulse-radiolysis study. *J Phys Chem* 95(9):3639–3643.
26. Candeias LP, Steenken S (1993) Electron transfer in di(deoxy)nucleoside phosphates in aqueous solution: Rapid migration of oxidative damage (via adenine) to guanine. *J Am Chem Soc* 115(6):2437–2440.
27. Page CC, Moser CC, Chen XX, Dutton PL (1999) Natural engineering principles of electron tunnelling in biological oxidation-reduction. *Nature* 402(6757):47–52.
28. Gray HB, Winkler JR (2005) Long-range electron transfer. *Proc Natl Acad Sci USA* 102(10):3534–3539.
29. Balland V, Byrdin M, Eker APM, Ahmad M, Brettel K (2009) What makes the difference between a cryptochrome and DNA photolyase? A spectroelectrochemical comparison of the flavin redox transitions. *J Am Chem Soc* 131(2):426–427.
30. Defelippis MR, et al. (1991) Electrochemical properties of tyrosine phenoxy and tryptophan indolyl radicals in peptides and amino acid analogs. *J Phys Chem* 95(8):3416–3419.
31. Seidel CAM, Schulz A, Sauer MHM (1996) Nucleobase-specific quenching of fluorescent dyes. 1. nucleobase one-electron redox potentials and their correlation with static and dynamic quenching efficiencies. *J Phys Chem* 100(13):5541–5553.
32. Woiczikowski PB, Steinbrecher T, Kubař T, Elstner M (2011) Nonadiabatic QM/MM simulations of fast charge transfer in *Escherichia coli* DNA photolyase. *J Phys Chem B* 115(32):9846–9863.
33. Sumi H, Marcus RA (1986) Dynamical effects in electron transfer reactions. *J Chem Phys* 84(9):4894–4914.
34. LeBard DN, Kapko V, Matyushov DV (2008) Energetics and kinetics of primary charge separation in bacterial photosynthesis. *J Phys Chem B* 112(33):10322–10342.